ACS APPLIED MATERIALS & INTERFACES

Research Article

www.acsami.org

Development of Sol–Gel Icephobic Coatings: Effect of Surface Roughness and Surface Energy

Qitao Fu,[†] Xinghua Wu,[†,‡] Divya Kumar,[†] Jeffrey W. C. Ho,[†,‡] Pushkar D. Kanhere,[‡] Narasimalu Srikanth,[‡,§] Erjia Liu,[§] Peter Wilson,[∥] and Zhong Chen*[,†,‡]

[†]School of Materials Science and Engineering and [§]School of Mechanical and Aerospace Engineering, Nanyang Technological University, 50 Nanyang Avenue, Singapore 639798

[‡]Energy Research Institute at NTU (ERI@N), 1 CleanTech Loop, #06-04, CleanTech One, Singapore 637141

[∥]Faculty of Health Sciences, University of Tasmania, Tasmania 7000, Australia

Supporting Information

ABSTRACT: Sol–gel coatings with different roughness and surface energy were prepared on glass substrates. Methyl triethoxysilane (MTEOS), 3-Glycidyloxypropyl trimethoxysilane (GLYMO) and fluoroalkylsilane (FAS) were used to obtain a mechanically robust icephobic coating. Different amount of hydrophobic silica nano particles was added as fillers to introduce different roughness and surface energy to the coatings. The microstructure, roughness, and surface energy, together with elemental information and surface chemical state, were investigated at room temperature. The contact angle and sliding angle were measured at different temperatures to correlate the wetting behavior at low temperature with the anti-icing performance. The ice adhesion shear strength was measured inside an ice chamber using a self-designed tester. The factors influencing the ice adhesion were discussed, and the optimum anti-icing performance found in the series of coatings. It was found that lower surface energy leads to lower ice adhesion regardless of the roughness, while the roughness plays a more complicated role. The wetting behavior of the droplet on surface changes as temperature decreases. The anti-icing performance is closely related to the antiwetting property of the surfaces at subzero temperatures.

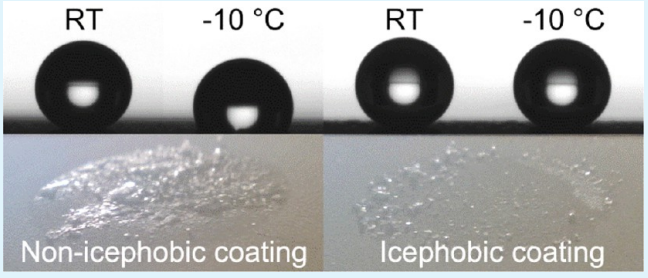

KEYWORDS: *sol–gel coating, icephobicity, ice adhesion, surface roughness, surface energy, mechanical durability*

INTRODUCTION

Ice accumulation can be a serious problem for the performance of outdoor structures, such as pavements, aircrafts, ships, locks and dams, offshore platforms, solar panels, power lines, etc. Ice formation can either lower the performance of the devices, or lead to total dysfunction of the whole equipment and system and result in great disasters in some cases. For example, the power loss because of ice accretion on wind turbines can reach up to 50% of the annual power production for certain locations.[1] The ice accumulation on power lines resulted from icy rain can cause the mechanical failure of the lines or collapse of power transmission towers, and resulted in serious electricity blackouts as happened in Southern China in early 2008.[2]

People have been trying to solve the ice accumulation problem for a long time. A lot of methods have been attempted, including heating, applying chemicals, using flexible materials, and coating a thin layer of organic materials, etc. However, most of them have their limitations, such as additional cost, efficiency, durability, and environmental problems.[3] New coatings that are mechanical robust and durable are needed to eliminate the limitations of the traditional anti-icing methods, and intensive research has been carried out in recent decades.

There are mainly two approaches leading to icephobic coatings. One incorporates a hydrophilic component into the coating. The absorbed water forms a thin lubricating film between ice and substrate so that the ice adhesion is significantly reduced.[4,5] One of such reports found that the low ice adhesion can be maintained for temperatures as low as −53 °C.[5] The other approach makes use of the conventional superhydrophic surfaces which usually show good self-cleaning property. This kind of coating can be achieved either by roughening a hydrophobic surface or decorating a rough surface with a low surface energy layer. In many cases, lithography[6−8] has been used for the fabrication of rough surfaces because of its ability to accurately control the surface morphology. This method, however, has its limitations, such as complicated procedure and high cost. In some other cases, chemical etching[9−11] was used especially for metal substrates, and thus set a limit for the choice of substrate and has additional

Received: July 3, 2014
Accepted: November 10, 2014
Published: November 10, 2014

constraint for large scale application. There are also other processes utilized for production of superhydrophobic and icephobic surfaces like laser irradiation,[12] liquid-infused porous surface,[13] chemical/physical vapor deposition,[14] etc. All these methods, however, either require special equipment or have high cost and potential mechanical limitations, rendering them unsuitable for mechanically robust, large scale applications. In contrast, sol−gel coatings, with the ability of easily adjusting surface energy and roughness through different precursors, surface decoration with self-assembled layers, addition of fillers of different sizes, etc.,[15−17] are a more promising way to develop large scale, mechanically durable, easy to apply, and low-cost superhydrophobic and icephobic coatings that can be applied in a wide range of substrates.

There are quite a number of sol−gel coatings developed to achieve superhydrophobicity or self-cleaning performance. However, there are limited investigations on the use of sol−gel coatings for icephobic purpose. It might be tempting to simply correlate self-cleaning with icephobicity because water repellence seems to be a common requirement for both. However, it has been shown that superhydrophobic materials do not always display good anti-icing performance.[18−22] Generally, icephobic coatings should display delayed ice formation, as well as reduced adhesion once the ice is formed. As far as the coating surface is concerned, there are mainly two factors that are related to its icephobic performance, which are the roughness and surface energy. Their roles in the anti-icing performance have been investigated in some literature.[19,23−28] Certain points have been well-accepted such as lower surface energy is favorable for better anti-icing performance.[19,28] However, usually very limited range of roughness was involved in previous reports and sometimes the investigations were not properly carried out. Ice nucleation is a process which happens at subzero temperatures. Thus, icephobicity is supposed to be more directly related to the wetting behavior of surfaces at low temperatures while this point was ignored by many authors, which might have contributed to the controversial conclusions in the past. There are a number of reports about the wetting behavior of surfaces at low temperatures, covering surfaces from superhydrophilic to superhydrophobic.[21,23,24,29,30] However, the investigations on the role of roughness and surface energy usually lack coherence between different samples, and sometimes the characterization methods were different from each other which makes it difficult for summary and comparison between each other. As a result, it remains unclear how these two factors affect the final anti-icing performance of surfaces. It is necessary to have a comprehensive investigation on the correlation between wettability and icephobicity especially at low temperatures. This forms the motivation of current work.

In this paper, a series of sol−gel coatings based on methyl triethoxysilane (MTEOS), 3-glycidyloxypropyl trimethoxysilane (GLYMO) and 1H, 1H, 2H, 2H-perfluorodecyltriethoxysilane (FAS) were developed. MTEOS was used as the cross-linker, GLYMO the coupling agent, and FAS the functional group to lower the surface energy of the base gel. Different content of hydrophobic silica particles were added as fillers to introduce different roughness to the surfaces as well as the surface energy. Surface roughness and apparent surface energy of the coatings were reported and correlated with the measured ice adhesion strength as a measurement of icephobicity.

EXPERIMENTAL SECTION

Preparation of Samples. Two group of coatings with different roughness and surface energy were prepared. The common sol for both groups were prepared as follows. 9.961 mL MTEOS (99%, Sigma-Aldrich, USA) and 33.132 mL GLYMO (≥98%, Sigma-Aldrich, USA) were mixed in 3.91 mL Ethanol (absolute for analysis, EMD Millipore Corporation, Germany) under stirring, and then 5.406 mL deionized (DI) water was added to the solution dropwise. After 1 h stirring, 3.55 g of itaconic acid (≥99%, Sigma-Aldrich, USA) was added to the solution to catalyze the hydrolysis process. The molar ratio of MTEOS, GLYMO, ethanol and water is 1:3:1.34:6.

After stirring for 1 h, solutions with different content of silica particles were prepared. The first group of solutions was prepared as follows. Hydrophobic fumed silica particles (AEROSIL R972, 16 nm, Nippon AEROSIL Co. Ltd., Japan) were first dispersed in ethanol (each gram of silica in 15 mL ethanol), and ultrasonically treated for half an hour to disperse the nanoparticles. The common sol was then added to the silica-containing ethanol to make solutions with a different weight percentage of silica particles. The final coatings contain 5, 10, 15, and 20 wt % silica particles, respectively. These samples are denoted as M-x where x stands for the weight percentage silica content in the coatings (Table 1). The second group of solutions

Table 1. Coating Compositions

sample ID	content of fumed silica filler in the final coating (wt %)	FAS content in the sol (μmol/g)
M-5	5	0
M-10	10	0
M-15	15	0
M-20	20	0
F-4	4	0.31−0.35
F-8	8	0.31−0.35
F-12	12	0.31−0.35
F-16	16	0.31−0.35

with FAS were prepared similarly, except that part of the ethanol for dispersing silica particles was replaced by FAS (97%, Sigma-Aldrich, USA) and DI water. The molar ratio of added FAS, DI water and MTEOS in the common sol was kept at 1:3:2 in all solutions of this group in order to make sure the base gel have the same surface energy. However, because of the difference in the amount of added fumed silica, the intrinsic surface energy of the final coatings may differ. This group of samples are named as F-y where y is the percentage of added silica in the final coating as shown in Table 1. Assuming all the FAS remains in the coating after calcination, the same amount of silica filler per unit of sprayed solution will lead to slightly decreased silica percentage in the FAS-containing coatings. However, by keeping the same amount of silica in the (unit volume) coating solution was found to keep similar roughness of the coatings, which will be reported later.

The finally mixed solutions were stirred for another 48 h for better hydrolysis before they were spray-coated onto glass slides. The glass substrate were cleaned with acetone, ethanol and DI water in sequence, and dried with hot air. After the spray coating, the samples were dried at room temperature for 1 h, followed by curing at 120 °C for another hour. For comparison, FAS monolayer decorated glass slide (without the sol−gel coating) was prepared as well. The decoration process is shown in the Supporting Information.

Materials Characterization. The roughness of the surfaces ware measured by a Surface Profiler (Alpha-Step IQ Surface Profiler, KLA Tencor). The surface morphology and elemental analysis were examined using a field emission scanning electron microscope (FESEM, JEOL JSM-6340F, Japan) and attached energy dispersive X-ray (EDX) spectroscopy. FTIR spectra were measured on a Frontier FTIR spectrometer (PerkinElmer Inc.). The contact angle and sliding angle at different temperatures, and the apparent surface energy of the samples at room temperature were measured with an OCA20 contact angle device (Dataphysics, Germany). In order to avoid a deformed

shape of the water droplet during the contact angle measurement, 4 μL of DI water was used to make sure its dimension is smaller than the capillary length which is around 2.7 mm for water at room temperature. The sliding angles were measured with 4 and 10 μL droplets, respectively. All the measurements were conducted at least 5 times for each sample. As for the surface energy measurement, DI water, glycerol and diethylene glycol were used, and the Owens, Wendt, Rabel and Kalble (OWRK) method was utilized for the calculation.

The ice adhesion was measured with a self-designed adhesion tester which consists of a weather chamber, an air compressor, an air cylinder combined with a force gauge on the tip of the pole, and a customized sample stage, as shown in Figure 1. The moving speed of the piston

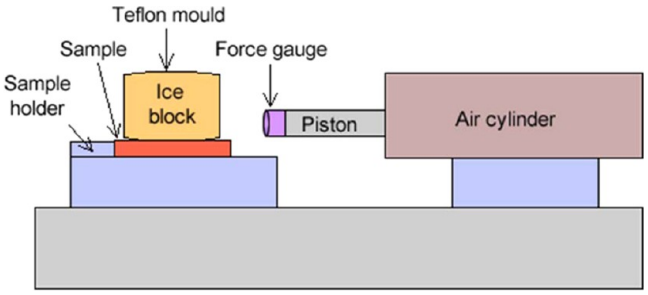

Figure 1. Schematic of ice adhesion tester.

was around 1.3 mm/s before it touched the ice mold. After the contact was established, the push force, driven by compressed air, increased at a rate of 12.5 N/s until the ice was sheared off. The data recording of the force gauge was conducted at 1000 records per second. The ice was formed in a customized Teflon mold which has an inner diameter of 18 mm, and a slope opening to minimize the adhesion between Teflon itself and the coatings. The mold was first filled with DI water, covered by the coatings, turned upside down, and then left in the weather chamber at −10 °C for at least 3 h to ensure the ice formation. The force F needed to push the mold off the coatings was recorded. The stand-off height was 0.5 mm during the shear test. The ice adhesion strength in shear can be calculated by

$$\tau = \frac{F}{A} \quad (1)$$

where $A = \pi \times 9^2$ mm^2 is the contact area between ice and the coatings in current study. The ice adhesion on bare glass and FAS decorated glass was also tested for comparison. The ice adhesion was measured at least 8 times on the same spot for each sample to get authentic results as well as to test the durability of the coatings.

RESULTS AND DISCUSSION

The surface morphology of the two groups of coatings are shown in Figure 2.

From the FESEM images, it can be clearly seen that the particles were dispersed well in the coatings. And the two groups of samples show similar surface morphology. As the content of silica particles reaches above 10 wt %, the surface becomes rougher, and starts to form a hierarchical structure with nanosized pores. The trend of the roughness increases with silica content is shown in Figure 3, and detailed data (root-mean-square, rms) are given in Table 2.

The contact angle and sliding angle of the samples, measured from room temperature (RT) down to −10 °C, are shown in Figure 4. Detailed data are reported in the Supporting Information, Table S1.

As seen in Figure 4, the contact angle of the coatings increases with the roughness. In the first group of samples (M series, without FAS addition), the contact angle at room temperature can reach up to 164.4°, and sliding angle around 8 and 3° for 4 and 10 μL droplet respectively, which indicates a Cassie wetting mode. However, when the temperature decreases, all the contact angles would decrease because of the condensation of vapor on the sample surface. And the superhydrophobic sample M-20 immediately loses its superhydrophobicity and becomes fully wetted as the droplets would not slide off the surface even when the sample is tilted at 90°. The contact angle of the other coated samples also decrease as temperature goes down, but at a much slower rate or even nearly no change for the M-5 sample. This is because these samples (M-15, M-10, M-5) have better wetting at room temperature, and they would not change much when the vapor condenses at lower temperatures.

For FAS containing samples, they show much higher contact angle than their counterparts with similar roughness in the first group because of the introduction of the C−F functional group. As can be seen from the FTIR spectra in Figure 5b, samples F-4 and F-8 show a strong absorption peak at 1238 cm^{-1}, which corresponds to the stretching mode of the C−F bond.[31] For samples F-12 and F-16, the absorption peak is relatively weak because of the decreased amount of FAS-treated common sol in the solid coating content. However, as can be seen in Figure 6, the fluorine element can still be detected with EDX even for F-16, while there is no trace of fluorine in the sample M-20. The full elemental analysis for all the coatings is shown in the Supporting Information (Figure S1, Table S2).

The introduced C−F functional group in the base gel not only increases the contact angle of the coatings, but also improves the antiwetting performance especially at subzero temperatures, which is more related to the anti-icing performance of coatings. As can be seen in Figure 4b, the contact angle of FAS-containing coatings can reach up to 172.7° at room temperature with sliding angle of 0.8° for a 10 μL droplet and 1.7° for a 4 μL droplet. The contact angle decreases and sliding angle increases as temperature goes down similar to the M series. However, the slope for contact angle change is very small for all samples in this group, and the contact angle remains above 150° even at −10 °C for samples F-12 and F-16. Nevertheless, the increase of sliding angles for these two samples are different. For sample F-12, the sliding angle increases quite a bit as temperature goes down, and reaches up to around 68° at −10 °C for a 10 μL droplet (and no sliding for the 4 μL droplet). This suggests a Cassie−Wenzel mixed wetting mode. For sample F-16, the sliding angle increases only a little as temperature goes down, and remains below 10° at −10 °C, which shows a good Cassie wetting mode.

The ice adhesion strength is shown in Table 2 and Figure 7. Comparing the two groups of samples, it is noticed that for the samples with similar roughness, the lower the surface energy, the lower the ice adhesion. This observation applies to all the samples, and is in agreement with results obtained by other authors.[19,28]

Inspecting the first group of samples without the FAS addition, the ice adhesion strength increases from 0.44 MPa to above 1 MPa when the silica content increases from 5 to 20 wt %. Notice that the roughness has increased drastically with the silica addition. The ice adhesion strength of M-20, the one with the highest roughness in the series, is even higher than the one on glass substrate without coating. For a low silica content sample like M-5, the surface is relatively smooth, and its surface energy is much lower than the bare glass (Table 2). In such a case the ice adhesion on the coating is lower than on the bare

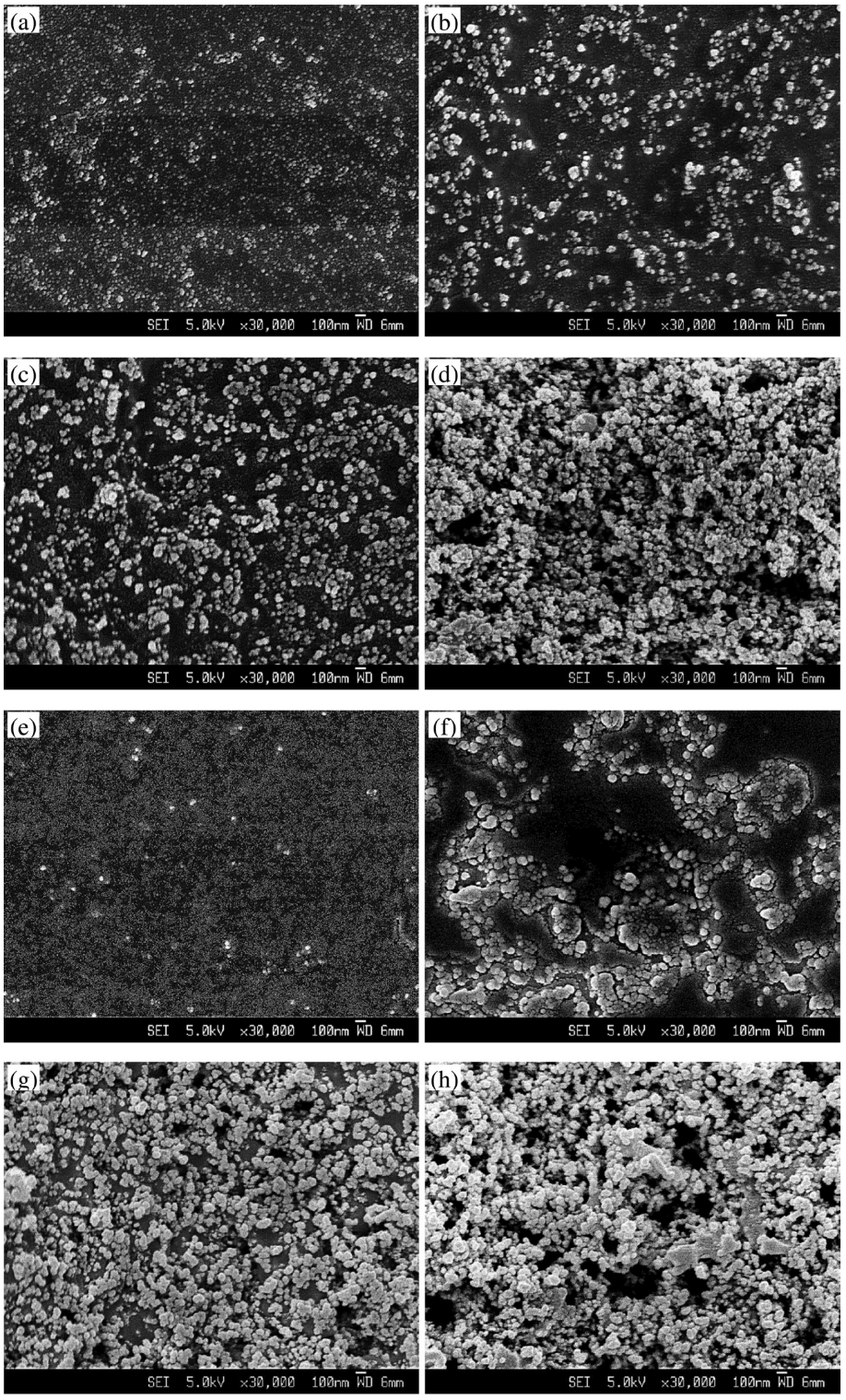

Figure 2. SEM micrographs showing the surface morphology of the coatings: (a) M-5, (b) M-10, (c) M-15, (d) M-20, (e) F-4, (f) F-8, (g) F-12, and (h) F-16.

glass, reflecting the effect of intrinsic lower surface energy. For this group of coatings, the intrinsic surface energy, which could probably be best estimated from the relatively flat M-5 sample, is around 31 mJ/m^2 (Table 2) or lower with more hydrophobic silica addition. Unfortunately we are not able to provide such an estimate when the roughness increases with more silica addition. For such (relatively) high surface energy coatings, the surface morphology plays a dominant role. With increasing silica content, none of the surfaces are able to keep the Cassie wetting mode at subzero degrees. This means that the highly roughened coatings were fully wetted and thus when the water freezes, it forms stronger bonding with the substrate because of the mechanical interlocking effect between the ice and substrate, leading to higher adhesion strength.[21,26,32,33] Under this circumstance, the rougher the surface, the greater the

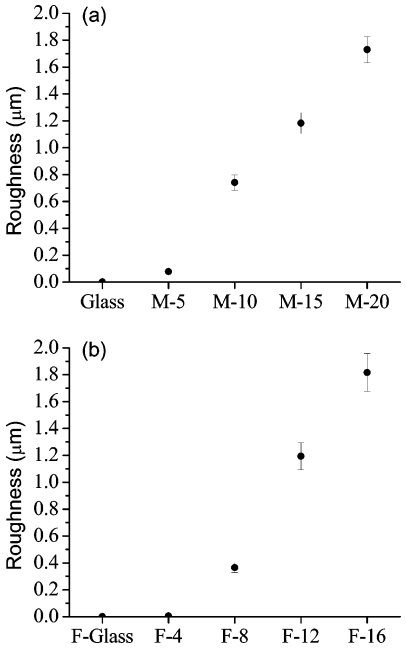

Figure 3. Surface roughness of coatings. (a) samples without addition of FAS; (b) samples with FAS.

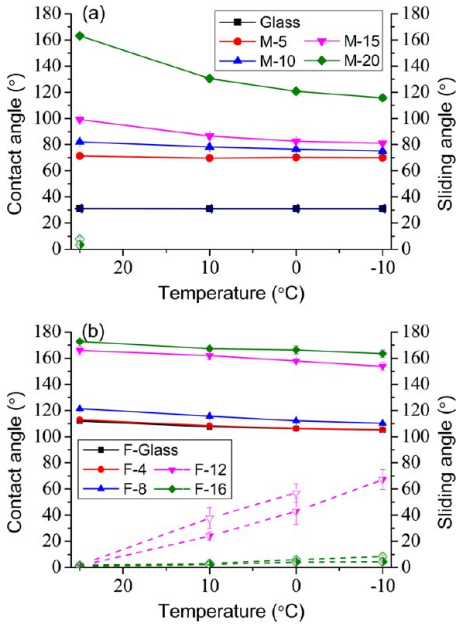

Figure 4. Water contact angle (solid symbol and line) and sliding angle (dashed line if applicable, open symbol for 4 μL droplet or half open symbols for 10 μL droplet) at different temperatures on (a) samples without FAS: only the M-20 sample displays water droplet sliding; (b) samples with FAS: F-12 and F-16 display water droplet sliding, whereas the others do not.

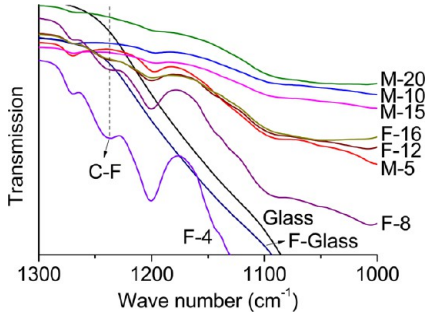

Figure 5. FTIR spectra of the samples.

anchor effect. That is why the ice adhesion on sample M-20 is the highest, even higher than the uncoated bare glass.

For the second group of samples with addition of FAS into the coating formulation, the surface energy decreases drastically. On the basis of the smooth sample F-4, the intrinsic surface energy is around 10 mJ/m^2, much lower than the M-series. Because of the low surface energy of the coating, the ice adhesion is lower than on the FAS decorated glass substrate. Referring to Figure 3b, both F-4 and F-glass have very low roughness compared with other samples in the group. As the content of the silica increases, the roughness increases, and the mechanical anchoring effect may start to influence the ice adhesion. This explains the slight increase in ice adhesion of F-8 sample. However, the ice adhesion strengths of all coated samples remain lower than on uncoated bare glass. For F-12 and F-16, the hierarchical porous coating structure with a hydrophobic base gel contributes to greater water repellence even at low temperatures. Although the sliding angle of F-12 rises to around 68 degrees at −10 °C (10 μL droplet), which likely indicates a Cassie−Wenzel mixed wetting mode with partially wetted surface, the remaining trapped air is still functional and contributes to the relatively lower ice adhesion than F-8 and F-4. The sliding angle of F-16 is 4.4° for the 10 μL droplet and 8.4° for the 4 μL droplet at −10 °C, which shows great superhydrophobicity and stable Cassie wetting mode at subzero temperature. This translates into the lowest ice adhesion strength at 0.075 MPa (Table 2).

The trapped air in the Cassie wetting mode may contribute in several ways to the good icephobic performance. First, it prevents the droplet to be in contact with the concave part of

Table 2. Surface Roughness, Apparent Surface Energy, and Ice Adhesion Strength

samples	roughness (rms, μm)	apparent surface energy (mJ/m^2)	disperse interaction (mJ/m^2)	polar interaction (mJ/m^2)	ice adhesion strength (MPa)
glass	0.001 ± 0.000	61.99	11.69	50.30	0.820 ± 0.096
M-5	0.078 ± 0.005	30.92	15.87	15.05	0.421 ± 0.053
M-10	0.741 ± 0.058	24.33	14.16	10.17	0.550 ± 0.107
M-15	1.183 ± 0.079	11.93	3.08	8.86	0.659 ± 0.099
M-20	1.730 ± 0.097	1.25	0.88	0.37	1.144 ± 0.214
F-Glass	0.001 ± 0.000	11.69	10.75	0.94	0.552 ± 0.062
F-4	0.006 ± 0.001	9.64	8.29	1.36	0.317 ± 0.082
F-8	0.365 ± 0.038	6.72	6.22	0.50	0.464 ± 0.073
F-12	1.194 ± 0.100	0.85	0.63	0.22	0.170 ± 0.066
F-16	1.817 ± 0.140	0.24	0.17	0.07	0.075 ± 0.019

dx.doi.org/10.1021/am504348x | ACS Appl. Mater. Interfaces 2014, 6, 20685−20692

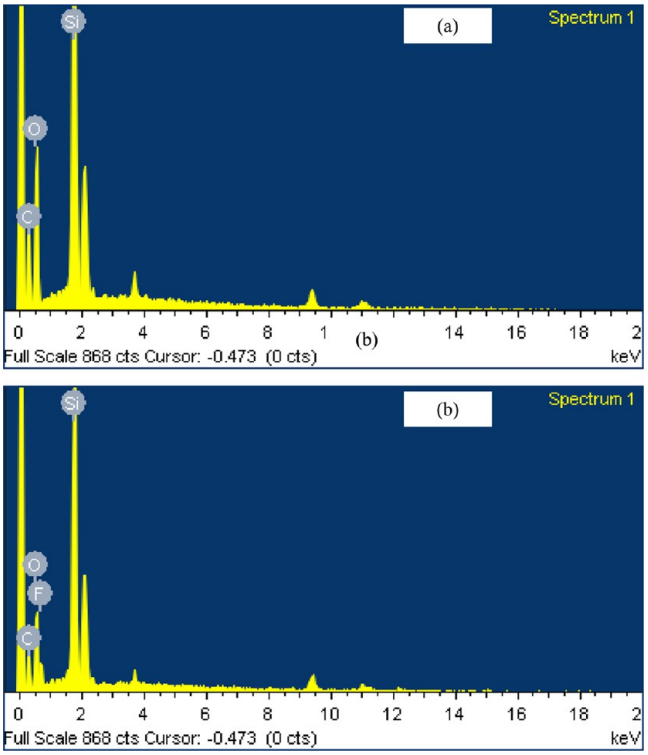

Figure 6. Element detection by EDX for samples (a) M-20 and (b) F-16.

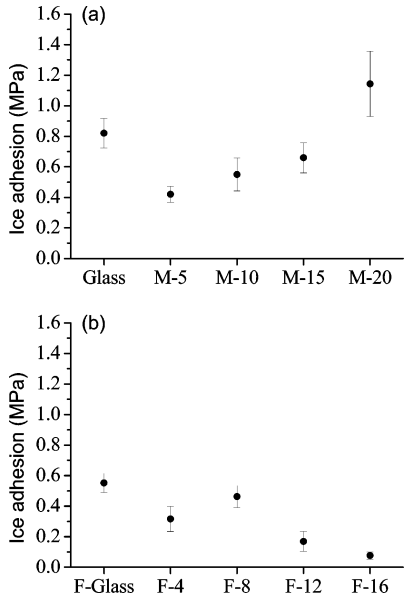

Figure 7. Ice adhesion strength of coatings (a) without FAS; (b) with FAS.

the asperities of the surface, i.e., the droplet can only lay on the top of the convex particles. According to the classical nucleation theory,[34−37] the heterogeneous nucleation is more difficult on a convex surface than on flat or concave surfaces.

Second, it reduces the contact area between ice and the coating surface, which minimizes the mechanical anchoring effect. According to Cassie's law,[38] the relationship between the apparent contact angle and surface feature can be described as

$$\cos\theta = f_1\cos\theta_1 + f_2\cos\theta_2 \quad (2)$$

where θ is the apparent contact angle, f_1 and f_2 the areal fraction of component 1 and 2, θ_1 and θ_2 the corresponding contact angle of component 1 and 2. When air is trapped, θ_2 = 180°, and $f_2 = 1 - f_1$, the equation reduces to $\cos\theta = f_1(\cos\theta_1 + 1) - 1$. For sample F-16, the apparent contact angle θ = 163.5° at −10 °C, and assuming the contact angle for a pure flat coating θ_1 is around 110°, then the fraction of the area contacting water is f_1 = 6.26%. Such low contact fraction, together with the minimized interlock effect, would decrease the ice adhesion dramatically. At the same time, it also minimizes the damage to the coating surface during ice removal, and thus helps maintain the coating durability.

Third, as the volume of water expands upon freezing, the trapped air in enclosure would be compressed and exert a counter-force on the ice block. This will reduce the ice adhesion to certain extent as well as make the structure of the formed ice at the interface less dense. As can be seen in Figure 8b, the residual ice crystals left after the adhesion test on sample F-16 are not many and very small, which indicates a loose ice structure at the interface between the ice block and the substrate. In contrast, there is usually a large fraction or full coverage of solid ice left on the Wenzel wetting mode rough surfaces because of the interlock effect (Figure 8a).

All these factors contribute to good durability of the icephobic coating as indicated by the narrow error bar of the ice adhesion strength on sample F-16 as shown in Figure 7b. The change of the shear strength with the number of icing/deicing cycles is shown in Figure S2 in the Supporting Information, and it can be seen clearly that the ice adhesion strength of F-16 does not change much during these cycles.

CONCLUSION

Two groups of samples with different surface energy and roughness were prepared and investigated. It was shown that the intrinsic surface energy and surface morphology of the coatings play important roles together. With only the addition of hydrophobic silica particles (M-series), the intrinsic surface energy is around 31 mJ/m^2, which is about half of the uncoated glass slide. In this series, low surface roughness combined with the reduced surface energy (e.g., M-5) leads to decreased ice adhesion compared with the uncoated bare glass. Increasing surface roughness by adding more silica particles increases the ice adhesion because of the interlocking effect. The addition of FAS reduces the intrinsic surface energy of the coating to around 10 mJ/m^2. Such low surface energy coatings are probably intrinsically icephobic. In such a case, increasing surface roughness enhances the icephobicity as indicated by the decreasing trend of ice adhesion strength.

This work has identified that not all superhydrophobic surfaces, as indicated by the water contact angle at room temperatures, could remain water repellent at low temperatures. Therefore, when correlating the water contact angle with icephobic performance, the angle should be measured at low temperatures. FAS could effectively reduce the surface energy of the base gel, and contributes to the superhydrophobicity at subzero temperatures. The trapped air between water and the superhydrophobic substrates can effectively reduce the ice adhesion and contribute to good durability of the icephobic coating. The best anti-icing performance was achieved on FAS dosed coating with 16 wt % silica, which has a sliding angle as low as 4.4° for a 10 μL droplet at −10 °C.

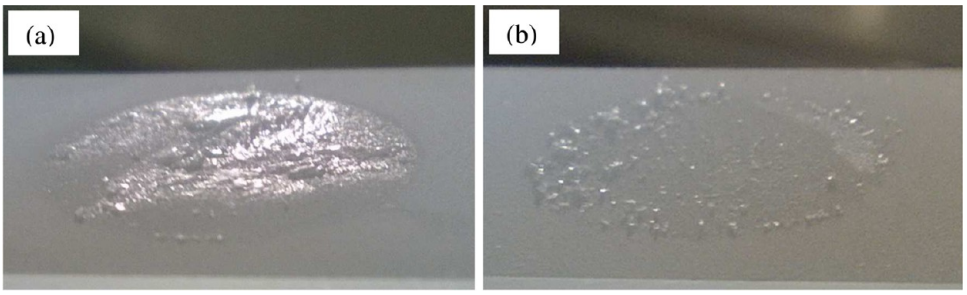

Figure 8. Residual ice after the adhesion test on sample (a) M-20, and (b) F-16.

■ ASSOCIATED CONTENT

Supporting Information

Preparation of FAS decoration on glass slides, detailed data of contact angles and sliding angles measured at different temperatures, elemental analysis of the coatings, and ice adhesion strengths on sample F-16 as a function of the number of icing/deicing cycles. This material is available free of charge via the Internet at http://pubs.acs.org.

■ AUTHOR INFORMATION

Corresponding Author

*E-mail: ASZChen@ntu.edu.sg.

Notes

The authors declare no competing financial interest.

■ ACKNOWLEDGMENTS

Q.T.F. and D.K. acknowledge the financial support from the Nanyang Technological University (NTU) in the form of a research scholarship. Z.C. acknowledges the SUG grant support from the College of Engineering (CoE) of NTU.

■ REFERENCES

(1) Parent, O.; Ilinca, A. Anti-Icing and De-Icing Techniques for Wind Turbines: Critical Review. *Cold Reg. Sci. Technol.* **2011**, *65*, 88–96.

(2) Li, T.; Li, J. Analysis of Icing Accident in South China Power Grids in 2008 and It's Countermeasures. In *20th International Conference and Exhibition on Electricity Distribution - Part 1, 2009 (CIRED 2009)* ; Prague, Czech Republic, June 8–11, 2009 ; IEEE: Piscataway, NJ, 2009.

(3) Lv, J. Y.; Song, Y. L.; Jiang, L.; Wang, J. J. Bio-Inspired Strategies for Anti-Icing. *ACS Nano* **2014**, *8*, 3152–3169.

(4) Chen, J.; Dou, R. M.; Cui, D. P.; Zhang, Q. L.; Zhang, Y. F.; Xu, F. J.; Zhou, X.; Wang, J. J.; Song, Y. L.; Jiang, L. Robust Prototypical Anti-Icing Coatings with a Self-Lubricating Liquid Water Layer between Ice and Substrate. *ACS Appl. Mater. Interfaces* **2013**, *5*, 4026–4030.

(5) Dou, R.; Chen, J.; Zhang, Y.; Wang, X.; Cui, D.; Song, Y.; Jiang, L.; Wang, J. Anti-Icing Coating with an Aqueous Lubricating Layer. *ACS Appl. Mater. Interfaces* **2014**, *6*, 6998–7003.

(6) Mishchenko, L.; Hatton, B.; Bahadur, V.; Taylor, J. A.; Krupenkin, T.; Aizenberg, J. Design of Ice-Free Nanostructured Surfaces Based on Repulsion of Impacting Water Droplets. *ACS Nano* **2010**, *4*, 7699–7707.

(7) Eberle, P.; Tiwari, M. K.; Maitra, T.; Poulikakos, D. The Rational Nanostructuring of Surfaces for Extraordinary Icephobicity. *Nanoscale* **2014**, *6*, 4874–4881.

(8) Maitra, T.; Tiwari, M. K.; Antonini, C.; Schoch, P.; Jung, S.; Eberle, P.; Poulikakos, D. On the Nanoengineering of Superhydrophobic and Impalement Resistant Surface Textures Below the Freezing Temperature. *Nano Lett.* **2013**, *14*, 172–182.

(9) Menini, R.; Farzaneh, M. Elaboration of Al_2o_3/Ptfe Icephobic Coatings for Protecting Aluminum Surfaces. *Surf. Coat. Technol.* **2009**, *203*, 1941–1946.

(10) Jafari, R.; Menini, R.; Farzaneh, M. Superhydrophobic and Icephobic Surfaces Prepared by Rf-Sputtered Polytetrafluoroethylene Coatings. *Appl. Surf. Sci.* **2010**, *257*, 1540–1543.

(11) Wang, F.; Li, C.; Lv, Y.; Lv, F.; Du, Y. Ice Accretion on Superhydrophobic Aluminum Surfaces under Low-Temperature Conditions. *Cold Reg. Sci. Technol.* **2010**, *62*, 29–33.

(12) Kietzig, A. M.; Mirvakili, M. N.; Kamal, S.; Englezos, P.; Hatzikiriakos, S. G. Nanopatterned Metallic Surfaces: Their Wettability and Impact on Ice Friction. *J. Adhes. Sci. Technol.* **2011**, *25*, 1293–1303.

(13) Wilson, P. W.; Lu, W.; Xu, H.; Kim, P.; Kreder, M. J.; Alvarenga, J.; Aizenberg, J. Inhibition of Ice Nucleation by Slippery Liquid-Infused Porous Surfaces (Slips). *Phys. Chem. Chem. Phys.* **2013**, *15*, 581–585.

(14) Wu, Y. Y.; Inoue, Y.; Sugimura, H.; Takai, O.; Kato, H.; Murai, S.; Oda, H. Characteristics of Ultra Water-Repellent Thin Films Prepared by Combined Process of Microwave Plasma-Enhanced Cvd and Oxygen-Plasma Treatment. *Thin Solid Films* **2002**, *407*, 45–49.

(15) Basu, B. J.; Hariprakash, V.; Aruna, S. T.; Lakshmi, R. V.; Manasa, J.; Shruthi, B. S. Effect of Microstructure and Surface Roughness on the Wettability of Superhydrophobic Sol-Gel Nanocomposite Coatings. *J. Sol–Gel Sci. Technol.* **2010**, *56*, 278–286.

(16) Textor, T.; Mahltig, B. A Sol-Gel Based Surface Treatment for Preparation of Water Repellent Antistatic Textiles. *Appl. Surf. Sci.* **2010**, *256*, 1668–1674.

(17) Lakshmi, R. V.; Bharathidasan, T.; Basu, B. J. Superhydrophobic Sol-Gel Nanocomposite Coatings with Enhanced Hardness. *Appl. Surf. Sci.* **2011**, *257*, 10421–10426.

(18) Farhadi, S.; Farzaneh, M.; Kulinich, S. A. Anti-Icing Performance of Superhydrophobic Surfaces. *Appl. Surf. Sci.* **2011**, *257*, 6264–6269.

(19) Zou, M.; Beckford, S.; Wei, R.; Ellis, C.; Hatton, G.; Miller, M. A. Effects of Surface Roughness and Energy on Ice Adhesion Strength. *Appl. Surf. Sci.* **2011**, *257*, 3786–3792.

(20) Varanasi, K. K.; Deng, T.; Smith, J. D.; Hsu, M.; Bhate, N. Frost Formation and Ice Adhesion on Superhydrophobic Surfaces. *Appl. Phys. Lett.* **2010**, *97*, 234102.

(21) Kulinich, S. A.; Farhadi, S.; Nose, K.; Du, X. W. Superhydrophobic Surfaces: Are They Really Ice-Repellent? *Langmuir* **2011**, *27*, 25–29.

(22) Karmouch, R.; Ross, G. G. Superhydrophobic Wind Turbine Blade Surfaces Obtained by a Simple Deposition of Silica Nanoparticles Embedded in Epoxy. *Appl. Surf. Sci.* **2010**, *257*, 665–669.

(23) Karmouch, R.; Ross, G. G. Experimental Study on the Evolution of Contact Angles with Temperature near the Freezing Point. *J. Phys. Chem. C* **2010**, *114*, 4063–4066.

(24) Heydari, G.; Thormann, E.; Järn, M.; Tyrode, E.; Claesson, P. M. Hydrophobic Surfaces: Topography Effects on Wetting by Supercooled Water and Freezing Delay. *J. Phys. Chem. C* **2013**, *117*, 21752–21762.

(25) Wang, Y.; Xue, J.; Wang, Q.; Chen, Q.; Ding, J. Verification of Icephobic/Anti-Icing Properties of a Superhydrophobic Surface. *ACS Appl. Mater. Interfaces* **2013**, *5*, 3370–3381.

(26) Hassan, M. F.; Lee, H. P.; Lim, S. P. The Variation of Ice Adhesion Strength with Substrate Surface Roughness. *Meas. Sci. Technol.* **2010**, *21*, 075701.
(27) He, M.; Li, H. L.; Wang, J. J.; Song, Y. L. Superhydrophobic Surface at Low Surface Temperature. *Appl. Phys. Lett.* **2011**, *98*, 093118.
(28) Petrenko, V. F.; Peng, S. Reduction of Ice Adhesion to Metal by Using Self-Assembling Monolayers (Sams). *Can. J. Phys.* **2003**, *81*, 387−393.
(29) Mockenhaupt, B.; Ensikat, H. J.; Spaeth, M.; Barthlott, W. Superhydrophobicity of Biological and Technical Surfaces under Moisture Condensation: Stability in Relation to Surface Structure. *Langmuir* **2008**, *24*, 13591−13597.
(30) Yin, L.; Xia, Q.; Xue, J. A.; Yang, S. Q.; Wang, Q. J.; Chen, Q. M. In Situ Investigation of Ice Formation on Surfaces with Representative Wettability. *Appl. Surf. Sci.* **2010**, *256*, 6764−6769.
(31) Simons, W. W. *Sadtler Handbook of Infrared Spectra*; Sadtler Research Laboratories: Philadelphia, 1978.
(32) Aoyama, T.; Ishikawa, M.; Hirata, T.; Ukigai, K. Effect of Surface Roughness on Adhesive Shear Strength between Pure Ice and a Solid Surface. *Trans. Jpn. Soc. Refrig. Air Cond. Eng.* **2011**, *23*, 273−281.
(33) Yang, S. Q.; Xia, Q. A.; Zhu, L.; Xue, J. A.; Wang, Q. J.; Chen, Q. M. Research on the Icephobic Properties of Fluoropolymer-Based Materials. *Appl. Surf. Sci.* **2011**, *257*, 4956−4962.
(34) Jamieson, M. J.; Nicholson, C. E.; Cooper, S. J. First Study on the Effects of Interfacial Curvature and Additive Interfacial Density on Heterogeneous Nucleation. Ice Crystallization in Oil-in-Water Emulsions and Nanoemulsions with Added 1-Heptacosanol. *Cryst. Growth Des.* **2005**, *5*, 451−459.
(35) Xu, D. H.; Johnson, W. L. Geometric Model for the Critical-Value Problem of Nucleation Phenomena Containing the Size Effect of Nucleating Agent. *Phys. Rev. B* **2005**, *72*, 052101.
(36) Cooper, S. J.; Nicholson, C. E.; Liu, J. A Simple Classical Model for Predicting Onset Crystallization Temperatures on Curved Substrates and Its Implications for Phase Transitions in Confined Volumes. *J. Chem. Phys.* **2008**, *129*, 124715.
(37) Fletcher, N. H. Size Effect in Heterogeneous Nucleation. *J. Chem. Phys.* **1958**, *29*, 572−576.
(38) Cassie, A. B. D.; Baxter, S. Wettability of Porous Surfaces. *Trans. Faraday Soc.* **1944**, *40*, 546−551.